chemistry proceedings

MDPI

Proceeding Paper

Construction of Lipid–Drug Conjugates for Beclomethasone Dipropionate

Shishuai Dang [1], Zhengwei Huang [2,*] and Xin Pan [1,*]

[1] School of Pharmaceutical Sciences, Sun Yat-sen University, Guangzhou 510006, China
[2] College of Pharmacy, Jinan University, Guangzhou 510632, China
* Correspondence: huangzhengw@jnu.edu.cn (Z.H.); panxin2@mail.sysu.edu.cn (X.P.)
† Presented at the 26th International Electronic Conference on Synthetic Organic Chemistry, 15–30 November 2022; Available online: https://ecsoc-26.sciforum.net/.

Abstract: Lipid-based nanoparticles (LBNs) are a new type of nanoparticulate drug-delivery system, which have gradually demonstrated broad prospects in pulmonary drug-delivery systems. However, the main disadvantage of these LBNs for inhalable drugs with limited lipophilicity is their low encapsulation capacity. Herein, this study anticipates establishing a technology platform to improve the loading capacity of low-lipophilicity drugs in LBNs for the therapy of lung diseases. A proof-of-concept study was carried out using Beclomethasone dipropionate (BDP) as a model drug. BDP was conjugated with stearic acid (SA), a kind of the lipid matrix for LBN. The conjugate was characterized and the interactions between the conjugate and SA were investigated via molecular dynamics simulation. It is expected that the drug-loading capacity of weak-lipophilic drugs in LBN can be increased by establishing the technology platform, and the application of LBNs in pulmonary delivery can be broadened.

Keywords: lipid-based nanoparticles; beclomethasone dipropionate; stearic acid; pulmonary administration

check for updates

Citation: Dang, S.; Huang, Z.; Pan, X. Construction of Lipid–Drug Conjugates for Beclomethasone Dipropionate. *Chem. Proc.* **2022**, *12*, 13. https://doi.org/10.3390/ecsoc-26-13528

Academic Editor: Julio A. Seijas

Published: 14 November 2022

Publisher's Note: MDPI stays neutral with regard to jurisdictional claims in published maps and institutional affiliations.

Copyright: © 2022 by the authors. Licensee MDPI, Basel, Switzerland. This article is an open access article distributed under the terms and conditions of the Creative Commons Attribution (CC BY) license (https://creativecommons.org/licenses/by/4.0/).

1. Introduction

Recently, nanoparticulate sustained release systems such as lipid-based nanoparticles (LBNs) have been attracting increasing interest. LBNs are drug-delivery systems based on surfactants-stabilized lipid matrices, including solid lipid nanoparticle (SLN), nanostructured lipid carriers (NLC), polymer–lipid hybrid nanoparticle (PLN) and liposome, etc. LBNs are versatile systems, and the application of LBN in the pulmonary drug delivery region has gradually shown broad prospects.

In pulmonary administration, the irritation of the drug-delivery system to the respiratory tract should always be considered during the formulation design. LBNs are composed of highly biocompatible lipid materials, which can significantly reduce the irritation to the respiratory tract [1]. This allows LBNs to fit the pulmonary drug-delivery system well [2]. At the same time, because the frequency of pulmonary drug administration greatly affects patient compliance, reducing the administration frequency through sustained-release technology has become an important research hotspot. From this stand point, as LBNs have an outstanding sustained-release effect [3], they enable us to reduce the frequency administration, resulting in improved patient compliance, which is essential in pulmonary administration therapy [4]. These attributes account for the popularity of LBNs in the field of pulmonary drug delivery.

However, there remains an important hurdle for the wider application of LBNs in pulmonary delivery. Many active pharmaceutical ingredients for pulmonary disease treatment are of low lipophilicity, including ambroxol hydrochloride, terbutaline sulfate, salbutamol sulfate and beclomethasone dipropionate (BDP). These low lipophilic drugs will show low encapsulation capacity in LBNs that consists of lipid materials [5], due to

'Like dissolves like' principles. This in turns indicates that the dosage should be raised or the dosing frequency should be increased. In this case, the aim of improving patient compliance cannot be achieved.

In response to this problem, this study anticipated establishing a technology platform that will improve the loading capacity of drugs with low lipophilicity in LBNs for pulmonary administration. A preliminary proof-of-concept study was carried out using BDP as a model drug.

In order to improve the loading capacity of BDP in LBNs, in this study, proper modification of BDP was performed based on the "Like dissolves like" principle. Stearic acid (SA) is one of the lipid matrices generally used for LBN, which has the advantage of good biocompatibility. A recent study even shows that elevated production of the anti-inflammatory cytokine interleukin-10 (IL-10) has been detected in stearic-acid-treated hepatocytes [6], which implies that stearic acid is capable of alleviation of inflammation. The modification by SA will expect low mucosal irritation and no toxic side effects in pulmonary delivery.

Therefore, BDP was conjugated with SA to be Lipid–Drug conjugate (LDC) called stearic acid–beclomethasone dipropionate conjugates (SA-BDP). With this method, the intensity of the interactions between the cargo and the lipid matrices are strengthened due to their similar structure. Through a stronger molecular interaction with the LBNs lipid matrix, the encapsulation capacity of BDP in LBNs could be enhanced. This study may provide a potential technology platform to improve the drug encapsulation ability of low-lipophilicity drugs in LBNs and broaden the application of LBNs in pulmonary delivery.

2. Materials and Methods

2.1. Materials

BDP was purchased from YuanYe Bio-Technology Co., Ltd. (Shanghai, China). The silica gel (200~300 mesh) for column chromatography and silica gel GF254 for thin-layer chromatography (TLC) was purchased from Lige Technology Co., Ltd. (Guangzhou, China). Stearoyl chloride, acetonitrile, methylene chloride, Boron fluoride ethyl ether, petroleum ether, and ethyl acetate were purchase from Aladdin Bio-Chem Technology Co., Ltd. (Shanghai, China).

2.2. Methods

2.2.1. SA-BDP Preparation

Synthesis. Figure 1 displays the synthesis pathway for preparing SA-BDP. All glass instruments and pipette tips were dried in a drying oven in advance for 24 h. Precisely 100 mg of BDP was weighed and dissolved in 4 mL of CH_2Cl_2/MeCN (50/50, *v*/*v*). Then, 100 µL of stearoyl chloride was added slowly. After complete dissolution, 100 µL of $BF_3 \bullet Et_2O$ was added. The reaction liquid and water were isolated throughout. Reactions were carried out at 0 °C for 2 h followed by 1 h of room temperature. The reaction was monitored with TLC.

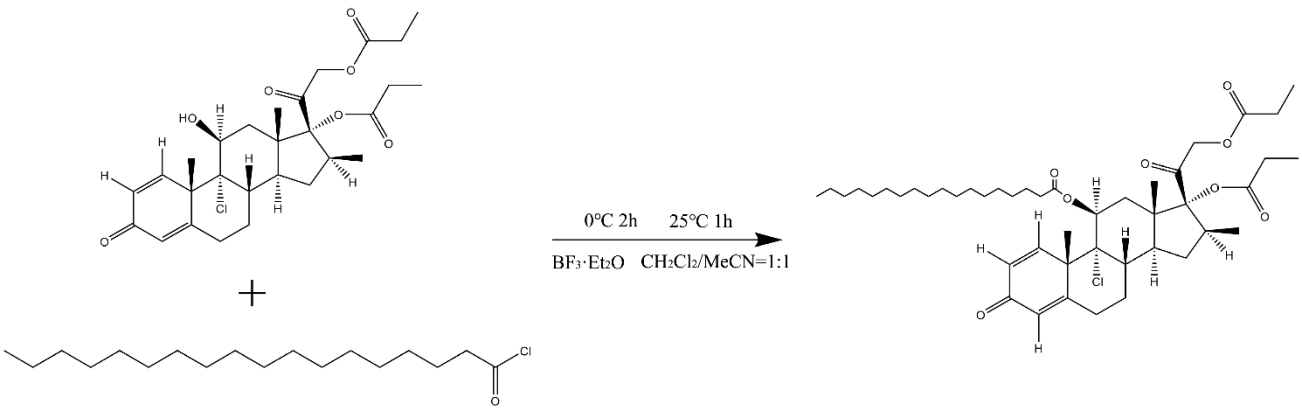


Figure 1. The synthetic route of SA-BDP.

Purifications. Solvents were removed under vacuum to complete dryness in a speed-vacuum dryer. They were then redissolved in 2 mL petroleum ether and ethyl acetate (5:1, v/v). Purification was performed using silica gel column chromatography with an elution volume of 50~70 mL (eluent system: petroleum ether: ethyl acetate = 5:1, v/v). The separation was monitored by TLC analysis. After high vacuum drying, ~30 mg of the product was obtained.

2.2.2. Characterization

Nuclear magnetic resonance (NMR). ^{1}H-NMR spectra were obtained with a NMR spectrometer (Bruker, AVANCE III HD 400 M, Germany) with spectrometer frequency offset of the first (observed) channel in 400.1324708 MHz. Spectra were obtained at a temperature of 25 °C, using zg30 pulse sequences, 10 µs pulse width, and 8196.722 spectral width, and the number of sampling points was 65,536. The relaxation duration was 1 s. The number of scans was 16. The time domain data were apodized with an exponential window function using a line broadening of 0.3 Hz.

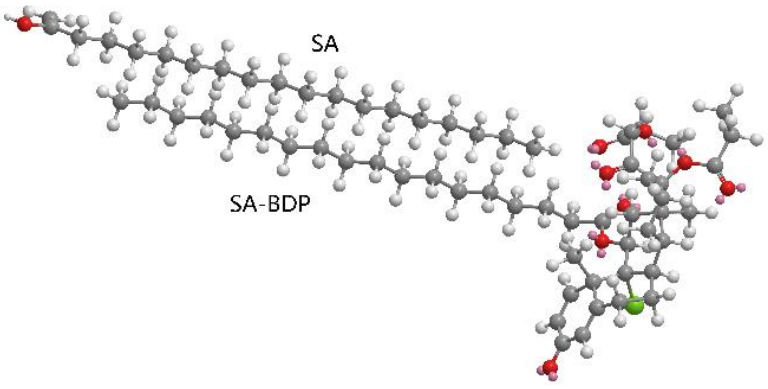
^{13}C-NMR spectra were obtained with a Bruker AVANCE III HD 400 M spectrometer with spectrometer frequency offset of the first (observe) channel in 100.6228298 MHz. Spectra were obtained at a temperature of 25 °C, using zgpg30 pulse sequences, 10 µs pulse width, 23,809.523 spectral width, and the number of sampling points was 65,536. The relaxation duration was 2 s. Number of scans was 1024. The time domain data were apodized with an exponential window function using a line broadening of 1.0 Hz.

Fourier Transform Infrared (IR). For FTIR analysis, 2 mg dried BDP/SA-BDP was properly mixed with 200 mg potassium bromide (KBr) and compressed to prepare a disc of about 3 mm in diameter. FTIR spectroscopy of the disc was recorded FTIR spectrometer (Thermo, Nicolet iS10, Waltham, MA, USA) at room temperature, in the frequency range of 400 to 4000 cm^{-1}, 32 scans per sample at a resolution of 4 cm^{-1}.

The X-ray diffraction (XRD). XRD pattern was recorded using an X-ray diffractometer (Rigaku, D8, Japan). The experimental parameters of the XRD experiment on the BDP/SA-BDP were as follows: A copper target (45 kV × 200 mA) was used at room temperature, with 2 × 106 cps of the linear range of the scintillation counter, and a step scanning method was used for data collection. Qualitative analysis using Bruker DIFFRAC.EVA V4.3 and refinement using Bruker DIFFRAC.TOPAS V6.0.

2.2.3. Molecular Dynamics Simulation

As the purpose of this work was to enhance BDP encapsulation efficiency in LBNs, the molecular dynamics simulation method was used to predict the drug-loading capacity of LBNs to SA-BDP. SA-BDP shared a similar structure with SA (the lipid matrices of LBNs), and it was anticipated that the interactions between SA-BDP and SA would be significantly stronger than those between BDP and SA. Figure 2 displayed the molecular structures of SA and SA-BDP, and the identical alkyl (C18) chain was highlighted.



.

Figure 2. The molecular structures of SA and SA-BDP.

In this study, the electrostatic force and van der Waals force were investigated. The reasons were as follows. The electrostatic interaction had a tuning effect on the stability of particles in solution and guided the self-assembly of the secondary structure. The van der Waals force was a weak interaction that generally existed among all molecules or atoms. These two interactions will help us to figure out the interactions between SA and SA-BDP, and between SA and BDP. Simulations for the electrostatic force and the van der Waals force between SA-BDP and SA were carried out using Gromacs-4.6.7 and compared with the electrostatic force between BDP and SA.

All the all-atom MD simulations were based on a GROMOS54a7 force field [7] created by ATB [8] and were carried out using the Gromacs-4.6.7 software package [9]. We used the relaxed system as a starting configuration. As it occurs prior to system relaxation MD, energy minimization was carried out with a composite protocol of steepest descent using termination gradients of 100 kJ/mol·nm. A 10 ns NPT relaxation was run at 298K for the equilibrium MD simulation. The Nosé–Hoover thermostat [10] was used to maintain the equilibrium temperature at 298 K and periodic boundary conditions were imposed on all three dimensions. The Particle Mesh–Ewald method [11,12] was used to compute long-range electrostatics within a relative tolerance of 1×10^{-6}. A cut-off distance of 1 nm was applied to real-space Ewald interactions. The same value was used for van der Waals interactions. The LINCS algorithm [9] was applied to constrain bond lengths of hydrogen atoms. A leap-frog algorithm [13] was used with a time step of 2 fs.

3. Results

Among the numerous lipid materials, SA is one of the most popular materials applied in sustained-release drug delivery [14]. Our goal was to obtain a modified product of BDP that had high drug-loading capacity if encapsulated in SA-based LBNs. For this purpose, BDP was conjugated with SA through a substitution reaction. This modification can improve the lipophilicity of the drug and enhance the interaction between the drug and the lipid material through structural similarity.

3.1. SA-BDP Preparation

The synthesis of SA-BDP was accomplished in a one-step reaction. This was similar to the reaction Radek Gazak et al. completed on silybin [15]. Interestingly, in that study, silybin had multiple hydroxyl groups and easily produced by-products, resulting in lower purity of the product. Meanwhile, in this study, BDP has only one hydroxyl group, and the reaction with SA would exhibit high selectivity and the amount of by-products might be negligible. The yield of the reaction is 14~27% (w/w). Compared with many other LDC synthesis methods [16,17], the reaction does not require heating, and has great potential in practical applications, particularly for thermolabile drugs.

In preliminary studies, a variety of separation methods have been considered, such as silica gel column chromatography, dextran gel column, molecular sieve chromatography, and thin-layer plate separation and extraction. Due to the poor water solubility of the reactants and products, and the susceptibility to acid/alkali degradation, the silica gel column chromatography separation was chosen. It was a method with high separation ability and easy operation, which has been widely used in the pharmaceutical industry [18]. Compared with commonly used vacuum distillation, vacuum drying can effectively prevent the drug from degradation under heat, remove the solvent more thoroughly, and is easier to transfer.

3.2. Characterization

We report the structural characterization of BDP (as reference) and SA-BDP. The molecular and crystal structures of both compounds are reported and discussed.

3.2.1. NMR

Figure 3A–D displayed the ^{1}H NMR spectra and ^{13}C NMR spectra of BDP and SA-BDP. The chemical shifts in NMR spectra were listed below.

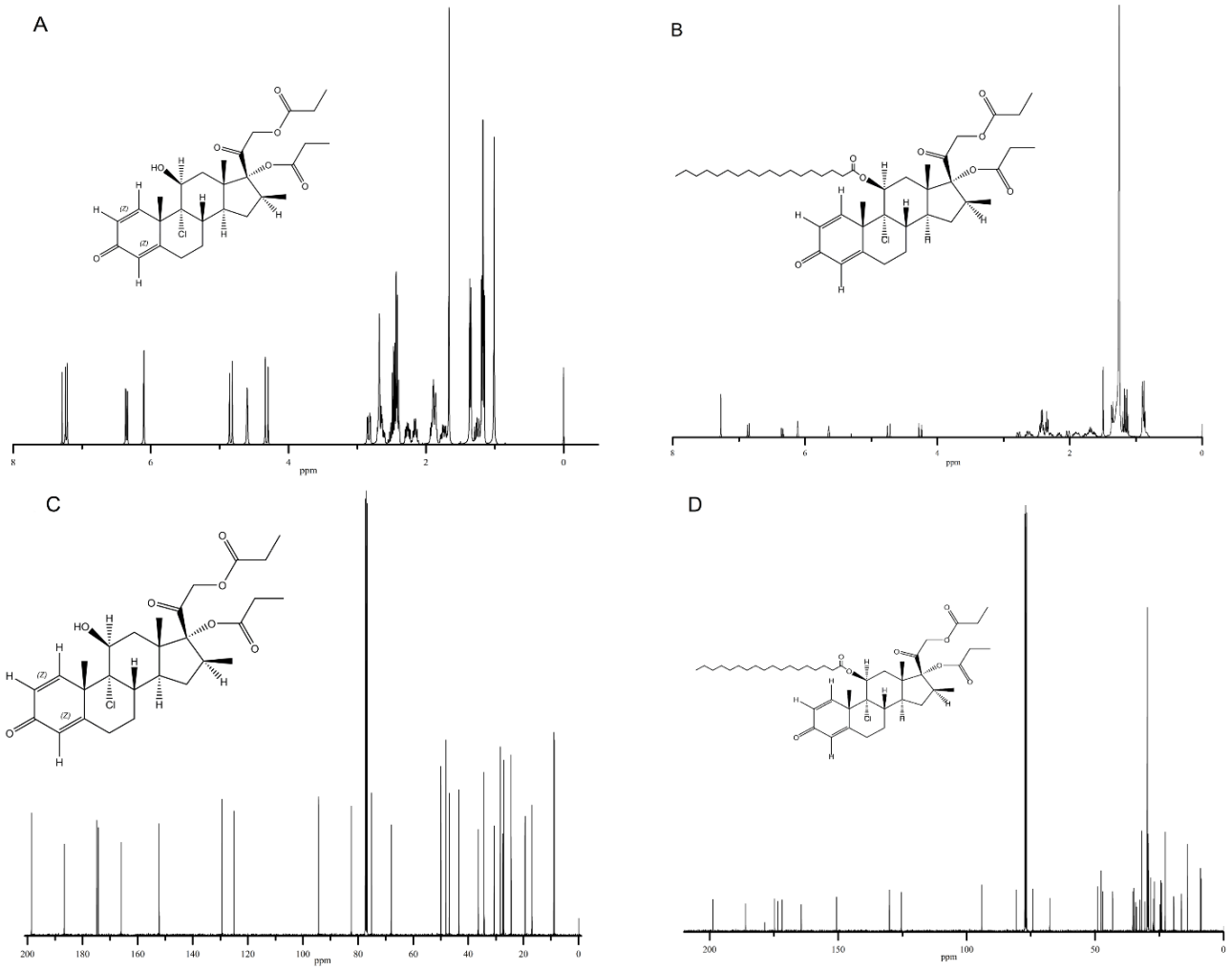


Figure 3. The ^{1}H-NMR spectra of BDP (**A**) and SA-BDP (**B**), and the ^{13}C-NMR of BDP (**C**) and SA-BDP (**D**).

BDP ^{1}H NMR (400 MHz, Chloroform-*d*) δ = 7.23 (d, *J* = 10.1 Hz, 1 H), 6.35 (dd, *J* = 10.1, 1.8 Hz, 1 H), 6.10 (s, 1 H), 4.84 (d, *J* = 16.4 Hz, 1 H), 4.60 (s, 1 H), 4.32 (d, *J* = 16.4 Hz, 1 H), 2.83 (dd, *J* = 14.1, 3.6 Hz, 1 H), 2.78–2.57 (m, 3 H), 2.56–2.34 (m, 5 H), 2.34–2.09 (m, 2 H), 1.99–1.83 (m, 3 H), 1.75 (m, *J* = 13.5, 11.7, 5.5 Hz, 1 H), 1.36 (d, *J* = 7.3 Hz, 3 H), 1.30–1.22 (m, 1 H), 1.17 (m, *J* = 7.5, 2.8 Hz, 6 H), 1.01 (s, 3 H).

BDP ^{13}C NMR (100 MHz, $CDCl_3$): δ = 198.5, 186.6, 174.8, 174.2, 165.9, 152.2, 129.4, 125.0, 94.3, 82.4, 82.4, 77.2, 75.1, 67.9, 49.9, 48.1, 46.9, 43.4, 36.4, 34.2, 34.2, 30.6, 28.3, 27.5, 27.1, 24.4, 19.4, 16.9, 8.9, 8.7.

SA-BDP ^{1}H NMR (400 MHz, Chloroform-*d*): δ = 6.86 (d, *J* = 10.1 Hz, 1 H), 6.34 (dd, *J* = 10.1, 1.8 Hz, 1 H), 6.11 (s, 1 H), 5.64 (s, 1 H), 4.74 (d, *J* = 16.4 Hz, 1 H), 4.26 (d, *J* = 16.3 Hz, 1 H), 2.78 (dd, *J* = 14.4, 3.7 Hz, 1 H), 2.62 (m, *J* = 18.4, 12.6, 12.0, 5.4 Hz, 2 H), 2.52–2.24 (m, 8 H), 2.16 (q, *J* = 8.0 Hz, 1 H), 2.03 (dd, *J* = 14.4, 2.6 Hz, 1 H), 1.91 (m, *J* = 18.4, 15.4, 5.5 Hz, 2 H), 1.83–1.58 (m, 4 H), 1.50 (s, 3 H), 1.36 (d, *J* = 7.4 Hz, 3 H), 1.16 (m, *J* = 15.4, 7.5 Hz, 6 H), 0.89 (dd, *J* = 11.6, 5.3 Hz, 8 H).

SA-BDP ^{13}C NMR (100 MHz, $CDCl_3$): δ = 198.7, 186.0, 178.6, 174.6, 173.5, 171.8, 164.3, 150.6, 130.0, 125.4, 94.1, 80.7, 77.2, 74.3, 67.6, 49.0, 47.7, 47.0, 43.1, 35.3, 34.9, 34.3, 33.9, 32.6,

31.9, 30.7, 29.7, 29.6, 29.6, 29.6, 29.6, 29.4, 29.4, 29.3, 29.2, 29.2, 29.0, 28.3, 27.3, 27.0, 24.7, 24.4, 24.1, 22.7, 19.3, 16.4, 14.1, 8.9, 8.8.

The main difference between the NMR spectra of BDP and SA-BDP was that after the modification of the SA fatty chain, the addition of hydrocarbyl hydrogen significantly reduces the original hydrogen intensity, but its position is basically unchanged, which indicates the success of the modification.

3.2.2. IR Spectra

Figure 4A,B summarized the IR spectra of BDP and SA-BDP.

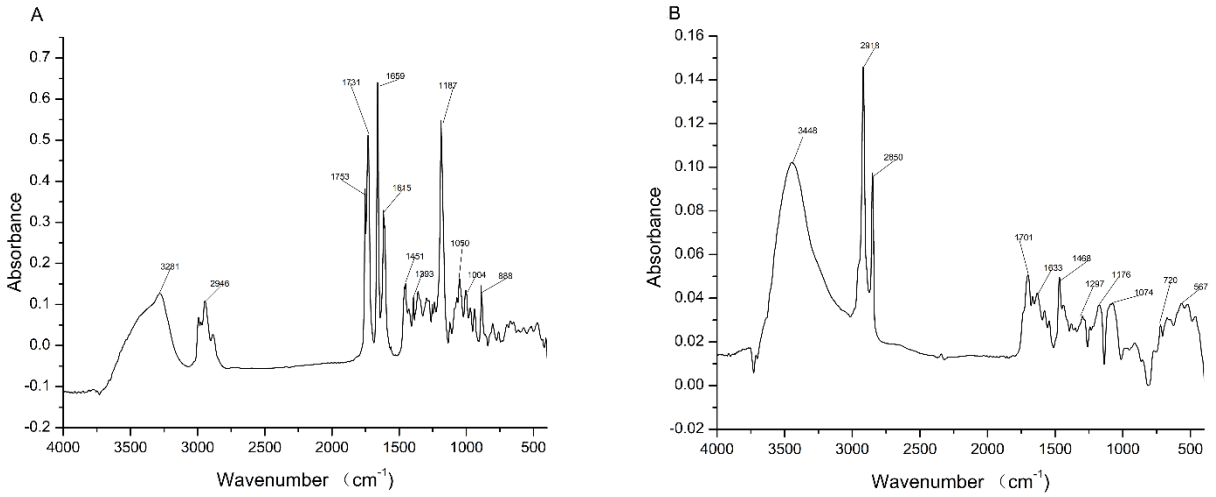


Figure 4. The IR spectra of BDP (**A**) and SA-BDP (**B**).

FT-IR analysis confirmed the presence of characteristic functional groups from BDP. The absorption at 3281 cm^{-1} was clearly due to the stretching vibration of the (–OH) groups. Meanwhile, the two absorption bands at 2946 cm^{-1} were observed, which were assigned to the antisymmetric and symmetric stretching vibration of the C-H in methyl or methylene. The absorption at 3010 cm^{-1} was due to the stretching vibration of the =C-H, the absorptions at 939 cm^{-1} and 888cm^{-1} were due to the wagging vibration of the=C-H, the absorption at 1753 cm^{-1} was due to the stretching vibration of the unconjugated C=O groups, the absorption at 1731 cm^{-1} was due to the stretching vibration of the C=O groups, the absorption at 1615 cm^{-1} and 1659 cm^{-1} was due to the stretching vibration of the C=C, the absorption at 1451 cm^{-1} and 1393 cm^{-1} was due to the bending vibration of the C-H, the absorption at 1187 cm^{-1} was due to the stretching vibration of the C-O in ester group, and the absorption at 1004 cm^{-1} and 1050 cm^{-1} was due to the stretching vibration of the C-O-C in the ester group.

The similar features in the IR spectra of the SA-BDP also showed the characteristic peaks. The two absorption bands at 2918 cm^{-1} and 2850 cm^{-1} were observed, which were assigned to the antisymmetric and symmetric stretching vibration of the C-H in methyl or methylene. The absorptions at 3010 cm^{-1} was due to the stretching vibration of the =C-H, and the absorptions at 1297 cm^{-1} and 1468 cm^{-1} were due to the bending vibration of the C-H. The absorption at 1701 cm^{-1} was due to the stretching vibration of the C=O groups, the absorption at 1633 cm^{-1} was due to the stretching vibration of the C=C, the absorption at 1176 cm^{-1} was due to the stretching vibration of the C-O in the ester group, the absorption at 1074 cm^{-1} was due to the stretching vibration of the C-O-C in the ester group, and the absorption at 720 cm^{-1} was due to the wagging vibration of the C-H, which showed there were long-chain alkyl groups in the sample.

The main difference between IR spectra of BDP and SA-BDP was that the 720 cm^{-1} peak appeared in the SA-BDP spectra, which was due to the wagging vibration of the C-H. This showed there were long-chain alkyl groups in the sample.

3.2.3. XRD

Figure 5A,B showed the XRD spectra of BDP and SA-BDP. BDP showed many characteristic peaks, which indicates that there are many crystal orientations, while SA-BDP exhibited fewer characteristic peaks, which means that the crystal orientation is relatively simple, indicating that SA-BDP is easier to form a single crystal. This might be attributed to the different lattice structures of BDP and SA-BDP.

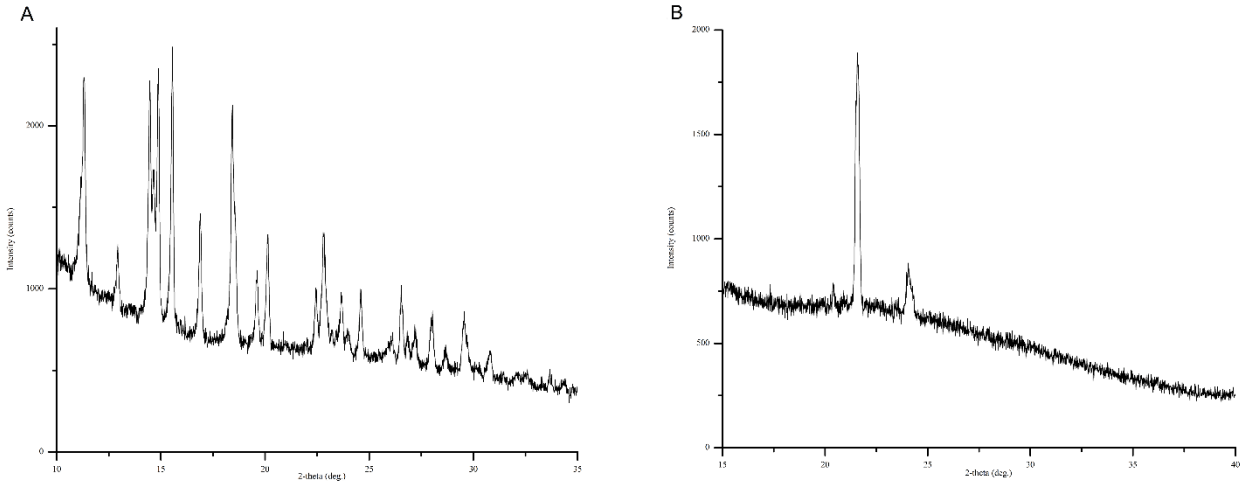


Figure 5. The XRD spectra of BDP (**A**) and SA-BDP (**B**).

Simulated XRD patterns were calculated with Bruker DIFFRAC.TOPAS V6.0 and compared with the experimentally observed pattern. Figure 6A,B showed the XRD refinement spectra of BDP and SA-BDP: fit data (red), test data (blue) and difference (green). The test data are consistent with the fitted data. The R-factor of weighted profile (Rwp) < 10%, indicating that the crystalline structures of BDP and SA-BDP are consistent with the prediction.

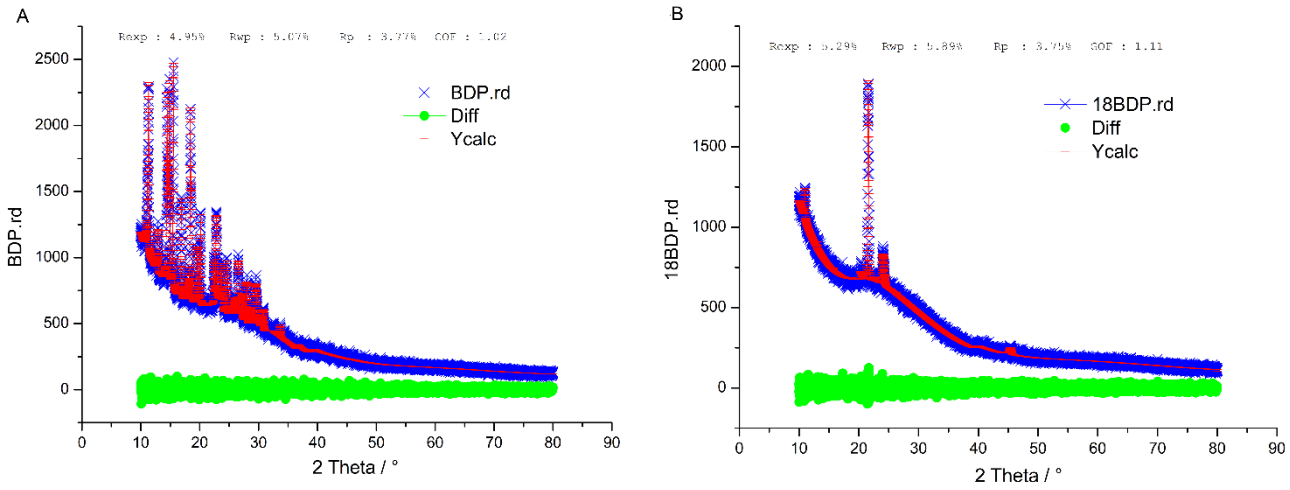


Figure 6. The XRD refinement spectra of BDP (**A**) and SA-BDP (**B**): fit data (red), test data (blue), difference (green).

By far, the differences in the NMR, IR, and XRD spectra of BDP and SA-BDP demonstrated that SA-BDP was successfully synthesized, and the related spectroscopic behaviours of SA-BDP were significantly different from BDP.

3.3. Molecular Dynamics Simulation

3.3.1. Electrostatic Force

Figure 7 showed the time evolution of the electrostatic force between two molecules in a water system.

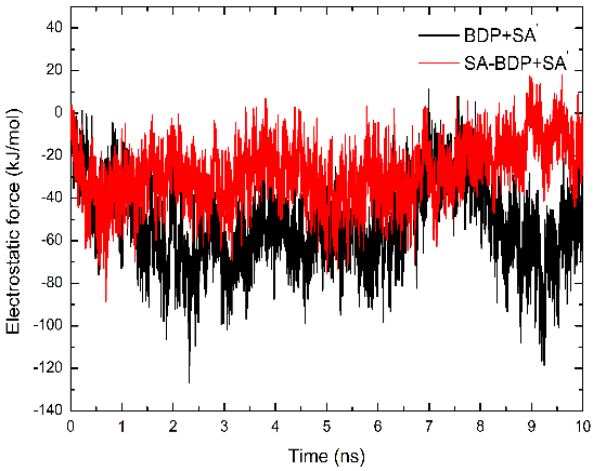


Figure 7. The electrostatic force between molecules changes with the simulation time of SA-BDP + SA (black) and BDP + SA (red).

It can be seen from Figure 7 that the electrostatic force between the two systems basically shows a dynamic balance, and the electrostatic forces of the two systems are relatively close. The electrostatic force depends on the size of the dipole moment of the polar group, the degree of orientation, the distance between the molecules, and the ambient temperature. The strength of the electrostatic force between the lipid matrix and the drug before and after modification is around 40 kJ/mol, which may be related to the small dipole moment of the lipid matrix and the limited modification of the drug's dipole moment.

3.3.2. Van Der Waals Force

Figure 8 showed how the time evolution of the van der Waals force between two molecules in a water system.

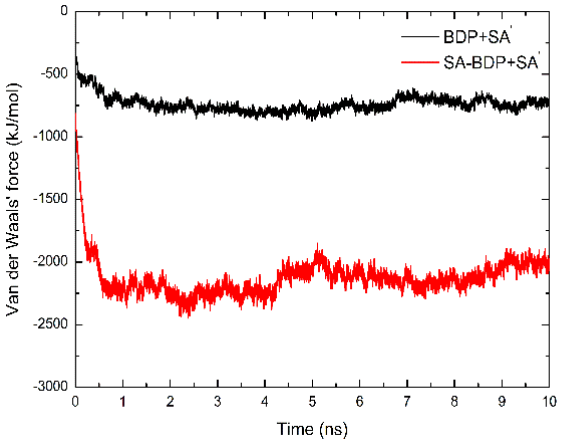


Figure 8. The Van der Waals force between molecules changes with the simulation time of SA-BDP + SA (black) and BDP + SA (red).

It can be seen from Figure 8 that the van der Waals interaction force between the two systems basically shows a dynamic balance, and the van der Waals interaction force between the two systems differs greatly. What needs illustrating is that the larger the

absolute value of electrostatic interaction or van der Waals interaction, the stronger the force. Therefore, the total interaction between SA-BDP and SA molecules is stronger than that between BDP and SA molecules. The van der Waals force between the modified drug and the lipid matrix is almost three times that before the modification. In addition to the principle of "Like dissolves like", this is due to the more dispersed electron cloud distribution of the modified drug and the increase in the intermolecular interaction area, which increases the dispersion force.

In summary, it is theoretically speculated that the electrostatic interaction between SA-BDP and SA was similar to that between BDP and SA, but the van der Waals force between SA-BDP and SA was stronger than that between BDP and SA. Therefore, SA-BDP and SA have stronger intermolecular interactions than BDP and SA. Due to the stronger molecular interaction between SA-BDP and SA, it can be predicted that the loading capacity of SA-BDP in LBNs will be desirable. The burst release effect of SA-BDP loaded LBNs might also be reduced. Further research will verify the real loading situation.

4. Discussion

In order to establish a technology platform to improve the loading capacity of drugs with undesirable lipophilicity in LBNs, we explored the feasibility of SA modification using BDP as a model drug, and finally showed that this modification is feasible and is expected to improve the loading capacity. A study on nicotine oral delivery also indirectly implies this [16]. In the future, we will expand the target drugs to ambroxol hydrochloride, terbutaline sulfate, salbutamol sulfate, etc. (these drugs for pulmonary disease therapy all have low lipophilicity), as they also contain hydroxyl groups in the molecular structure and a similar substitution reaction can be performed. Actually, due to the generality of hydroxyl groups in drug molecules, this technology platform possesses high potential for application.

Based on the BDP model, this study can not only build a technical platform, but also provides potential opportunities for asthma treatment. As the first-line treatment for asthma [19], the recommended dosage of BDP is 800 μg bid, and long-term prophylactic administration is required. A large number of studies have proved that frequent administration of drugs reduces patient compliance and thus affects the treatment effect [20–22]. After improving the loading efficiency of BDP in LBNs, the frequency of administration can be significantly reduced, and it will directly reduce the impact of long-term treatment on the patient's quality of life and avoid the psychological burden of the "patient" stereotype on the patient. From this perspective, this work may finally improve patient compliance and thus have a positive impact on the treatment of asthma.

Because of the long alkyl chain (C_{18}) structure of SA, the SA-BDP conjugate may even be able to self-assemble into a nanocrystalline drug-delivery system without relying on external lipids [23], and the feasibility of its self-assembly will be explored in the future.

Author Contributions: Conceptualization, S.D. and Z.H.; methodology, S.D.; software, S.D.; validation, S.D.; formal analysis, S.D.; investigation, S.D.; resources, S.D.; data curation, S.D.; writing—original draft preparation, S.D.; writing—review and editing, Z.H.; visualization, S.D.; supervision, X.P.; project administration, S.D.; funding acquisition, X.P. All authors have read and agreed to the published version of the manuscript.

Funding: This research was funded by the [Special Funds for the Cultivation of Guangdong College Students' Scientific and Technological Innovation ("Climbing Program" Special Funds)] under Grant [number pdjh2019a0003]; and [National Natural Science Foundation of China] under Grant [number 81673375; 81703431].

Institutional Review Board Statement: Not applicable.

Informed Consent Statement: Not applicable.

Data Availability Statement: The data presented in this study are available on request from the corresponding author.

Acknowledgments: The authors wish to thank Zhen Yang (RWTH Aachen University) and Hui Wang (Sun Yat-sen University) for their kind help with the synthetic experiments.

Conflicts of Interest: The authors declare no conflict of interest.

References

1. Aggarwal, A.N.; Kumari, R.; Grover, S. Patient Satisfaction With Inhaled Medication for Asthma. *Respir. Care* **2018**, *63*, 859–864. [CrossRef] [PubMed]
2. Astrakas, L.G.; Gousias, C.; Tzaphlidou, M. Structural destabilization of chignolin under the influence of oscillating electric fields. *J. Appl. Phys.* **2012**, *111*, 074702. [CrossRef]
3. Berendsen, H.J.C.; Postma, J.P.M.; Van Gunsteren, W.F.; DiNola, A.; Haak, J.R. Molecular dynamics with coupling to an external bath. *J. Chem. Phys.* **1984**, *81*, 3684–3690. [CrossRef]
4. Ding, Y.; Nielsen, K.A.; Nielsen, B.P.; Bøje, N.W.; Müller, R.H.; Pyo, S.M. Lipid-drug-conjugate (LDC) solid lipid nanoparticles (SLN) for the delivery of nicotine to the oral cavity–Optimization of nicotine loading efficiency. *Eur. J. Pharm. Biopharm.* **2018**, *128*, 10–17. [CrossRef] [PubMed]
5. Essmann, U.; Perera, L.; Berkowitz, M.L.; Darden, T.; Lee, H.; Pedersen, L.G. A smooth particle mesh Ewald method. *J. Chem. Phys.* **1995**, *103*, 8577–8570. [CrossRef]
6. Gažák, R.; Purchartová, K.; Marhol, P.; Živná, L.; Sedmera, P.; Valentová, K.; Kato, N.; Matsumura, H.; Kaihatsu, K.; Křen, V. Antioxidant and antiviral activities of silybin fatty acid conjugates. *Eur. J. Med. Chem.* **2010**, *45*, 1059–1067. [CrossRef] [PubMed]
7. Hess, B.; Kutzner, C.; van der Spoel, D.; Lindahl, E. GROMACS 4: Algorithms for Highly Efficient, Load-Balanced, and Scalable Molecular Simulation. *J. Chem. Theory Comput.* **2008**, *4*, 435–447. [CrossRef]
8. Ivanova, E.P.; Nguyen, S.H.; Guo, Y.; Baulin, V.A.; Webb, H.K.; Truong, V.K.; Wandiyanto, J.V.; Garvey, C.J.; Mahon, P.J.; Mainwaring, D.E.; et al. Bactericidal activity of self-assembled palmitic and stearic fatty acid crystals on highly ordered pyrolytic graphite. *Acta Biomater.* **2017**, *59*, 148–157. [CrossRef]
9. Jin, N.J.N.; Pyo, S.M.P.S.M.; Keck, C.M.; Müller, R.H. Maximum Loaded Amorphous Azithromycin Produced Using the Wetness Impregnation Method with Fractional Steps for Dermal Prophylaxis Against Lyme Disease. *Die Pharm.* **2019**, *74*, 345–349.
10. Juniper, E.F. The impact of patient compliance on effective asthma management. *Curr. Opin. Pulm. Med.* **2003**, *9*, S8–S10. [CrossRef]
11. Leifer, F.G.; Konicek, D.M.; Chen, K.-J.; Plaunt, A.J.; Salvail, D.; Laurent, C.E.; Corboz, M.R.; Li, Z.; Chapman, R.W.; Perkins, W.R.; et al. Inhaled Treprostinil-Prodrug Lipid Nanoparticle Formulations Provide Long-Acting Pulmonary Vasodilation. *Drug Res.* **2018**, *68*, 605–614. [CrossRef]
12. Lerata, M.S.; D'Souza, S.; Sibuyi, N.R.; Dube, A.; Meyer, M.; Samaai, T.; Antunes, E.M.; Beukes, D.R. Encapsulation of Variabilin in Stearic Acid Solid Lipid Nanoparticles Enhances Its Anticancer Activity in Vitro. *Molecules* **2020**, *25*, 830. [CrossRef] [PubMed]
13. Malde, A.K.; Zuo, L.; Breeze, M.; Stroet, M.; Poger, D.; Nair, P.C.; Oostenbrink, C.; Mark, A.E. An Automated Force Field Topology Builder (ATB) and Repository: Version 1.0. *J. Chem. Theory Comput.* **2011**, *7*, 4026–4037. [CrossRef] [PubMed]
14. Nishitani, Y.; Okazaki, S.; Imabayashi, K.; Katada, R.; Umetani, K.; Yajima, H.; Matsumoto, H. Saturated and monounsaturated fatty acids increase interleukin-10 production in rat hepatocytes. *Nihon Arukoru Yakubutsu Igakkai Zasshi* **2007**, *42*, 32–35. [PubMed]
15. Olbrich, C.; Gessner, A.; Kayser, O.; Müller, R.H. Lipid-Drug-Conjugate (LDC) Nanoparticles as Novel Carrier System for the Hydrophilic Antitrypanosomal Drug Diminazenediaceturate. *J. Drug Target.* **2002**, *10*, 387–396. [CrossRef]
16. Plaza, V.; Giner, J.; Calle, M.; Rytilä, P.; Campo, C.; Ribó, P.; Valero, A. Impact of patient satisfaction with his or her inhaler on adherence and asthma control. *Allergy Asthma Proc.* **2018**, *39*, 437–444. [CrossRef]
17. Puri, A.; Loomis, K.; Smith, B.; Lee, J.-H.; Yavlovich, A.; Heldman, E.; Blumenthal, R. Lipid-Based Nanoparticles as Pharmaceutical Drug Carriers: From Concepts to Clinic. *Crit. Rev. Ther. Drug Carr. Syst.* **2009**, *26*, 523–580. [CrossRef]
18. Reddel, H.K.; FitzGerald, J.M.; Bateman, E.D.; Bacharier, L.B.; Becker, A.; Brusselle, G.; Buhl, R.; Cruz, A.A.; Fleming, L.; Inoue, H. GINA 2019: a fundamental change in asthma management. Treatment of asthma with short-acting bronchodilators alone is no longer recommended for adults and adolescents. *Eur. Respir. J.* **2019**, *53*, 1901046. [CrossRef]
19. Rehman, A.; Amin, F.; Sadeeqa, S. Prevalence of asthma and its management: A review. *J. Pak. Med. Assoc.* **2018**, *68*, 1823–1827.
20. Schmid, N.; Eichenberger, A.P.; Choutko, A.; Riniker, S.; Winger, M.; Mark, A.; Van Gunsteren, W.F. Definition and testing of the GROMOS force-field versions 54A7 and 54B7. *Eur. Biophys. J.* **2011**, *40*, 843–856. [CrossRef]
21. Triolo, D.; Craparo, E.; Porsio, B.; Fiorica, C.; Giammona, G.; Cavallaro, G. Polymeric drug delivery micelle-like nanocarriers for pulmonary administration of beclomethasone dipropionate. *Colloids Surf. B Biointerfaces* **2017**, *151*, 206–214. [CrossRef] [PubMed]
22. Van Gunsteren, W.F.; Berendsen, H.J.C. A Leap-frog Algorithm for Stochastic Dynamics. *Mol. Simul.* **1988**, *1*, 173–185. [CrossRef]
23. Zielińska, A.; Ferreira, N.R.; Feliczak-Guzik, A.; Nowak, I.; Souto, E.B. Loading, release profile and accelerated stability assessment of monoterpenes-loaded solid lipid nanoparticles (SLN). *Pharm. Dev. Technol.* **2020**, *25*, 832–844. [CrossRef] [PubMed]